IET Microwaves, Antennas & Propagation

Research Article

IET Journals
The Institution of Engineering and Technology

V-band Bull's eye antenna for multiple discretely steerable beams

ISSN 1751-8725
Received on 3rd July 2015
Revised on 31st August 2015
Accepted on 12th October 2015
doi: 10.1049/iet-map.2015.0425
www.ietdl.org

Clement J. Vourch[1], *Timothy D. Drysdale*[2] ✉

[1]*Electronics and Nanoscale Engineering Division, University of Glasgow, Glasgow G12 8LT, UK*
[2]*Department of Engineering and Innovation, The Open University, Milton Keynes MK7 6AA, UK*
✉ *E-mail: timothy.d.drysdale@ieee.org*

Abstract: The authors present a new approach to designing V-band Bull's eye antennas so as to produce multiple beams, which are either fixed or discretely steerable. Bull's eye antennas comprise concentric rings around a subwavelength aperture. Beam deflection is accomplished by adjusting the effective spacing of the rings, which they explain in terms of the coupling angle to free space and surface waves. They show that multiple beams can be obtained from a single antenna, with the deflection of each beam being controlled independently by the relevant portion of the ring pattern. They demonstrate the principle through rigorous full-wave simulations of two-beam antennas with symmetrical and asymmetrical shifts, and give experimental results for a prototype milled in aluminium, with two separate fixed beams each deflected 16° to either side of the broadside. They also propose means to obtain up to six different beam arrangements during operation by mechanically rotating a plate containing a special six-sector ring pattern. Their simulated example gives three patterns, a single broadside beam or two beams each deflected by 8° or 15°. The radiation efficiency of the antenna is 97% and the gain of a single undeflected beam is 18.1 dBi.

1 Introduction

Bull's eye antennas were first used at optical wavelengths to enhance the transmission from subwavelength apertures associated with single-mode optical fibres, light-emitting diodes and semiconductor lasers [1]. The principle applies equally well to out-coupling from single-mode waveguides in the micro- and millimetre-wave bands. A millimetre-wave antenna based on this principle is of interest because it offers a very low profile and good directivity [2–4], yielding similar performance to a horn antenna for a fraction of the size. Compact, directive antennas are important where space and energy use are at a premium, for example, communicating between members of a swarm of small satellites or point-to-point communications within existing infrastructures. For convenience, the main beam should be able to be designed so that communication links can be established even when the sides of the small satellite or building walls are known not to be facing each other; split into multiple beams where simultaneous communication is desired with more than two parties, and/or steered to accommodate changes in the relative positions of the transmitter and the receiver. The possibility of changing the direction of the main beam by shifting the centre of the rings has been reported at optical frequencies [5] and at millimetre-wave frequencies [6–8]. This concept is called the holographic principle and allows beam steering and beam forming by scattering the surface currents with specific surface impedance patterns [9, 10]. In the case of the Bull's eye antenna, those patterns are periodic, metallic gratings. In our earlier work [6], we showed that shifting the rings deflects the main beam in both the *E*-plane and *H*-plane, but the amount of deflection was fixed for a given design and not adjustable after the antenna was manufactured.

In this paper, we extend our analysis of the shifting effect to show that it is consistent with the coupling angle between free-space waves and surface waves on a periodic grating. We exploit the localised nature of the leaky waves to extend the design to give multiple beams and discretely steerable single or multiple beams. Specifically, we experimentally demonstrate dual beam operation and propose and simulate a mechanical tuning scheme for live or 'on-the-fly' beam steering of one (or two beams) to six (or three) discrete angles. For consistency in presentation, we begin with the same antenna design that we used in [6].

The design dimensions of an antenna with a single beam emitted along the broadside are defined in Fig. 1, and listed in Table 1. Note that the antenna performance is insensitive to *G*, as long as the ground plane is large enough to contain the indented rings.

We assume the antenna is fed from the rear by a WR-15 rectangular waveguide, with the long side of the waveguide parallel to *L*. This gives operating frequencies that are centred about 60 GHz. The rectangular aperture results in a linear polarisation. A WR-15 feed is not the only possible option for this antenna, but since it is convenient for our experimental setup we do not explore other feed options in this paper.

A linearly polarised antenna is adequate for communications in the 60 GHz band because there is minimal Faraday rotation of the polarisation [11, 12]. In any case, atmospheric losses are high in the 60 GHz band, so we expect most uses of our antenna to be in short ground–ground or space–space communications links where Faraday rotation does not occur. Furthermore, linear polarisation is desirable from the point of view of enabling polarisation-based multiplexing for additional channel capacity.

Other antennas in the 60 GHz range achieve wide impedance bandwidth (33%) with modest gain (7.5 dBi) [13] or use arrays of dielectric resonators fed by substrate integrated waveguides [14] for increased gain (16.5 dBi). The use of dielectrics in such antennas reduces the radiation efficiency due to substrate losses in the complex waveguide networks, needed to feed enough antennas to form an array with high directivity. On the other hand, we anticipate that widespread adoption of 60 GHz communications systems will drive demand for alternative solutions that are efficient, with high gain, yet inexpensive and straightforward to manufacture.

This paper is organised as follows. In Section 2, we explain the operation of the antenna in terms of leaky waves, using as the example the *E*-plane shift of a single beam. In Section 3, we show how to achieve multiple beams and show that each of the beams in a two-beam design is individually deflectable. In Section 4, we present measurement results for a symmetrical double-shifted ring structure. We present the design of a mechanically steerable Bull's

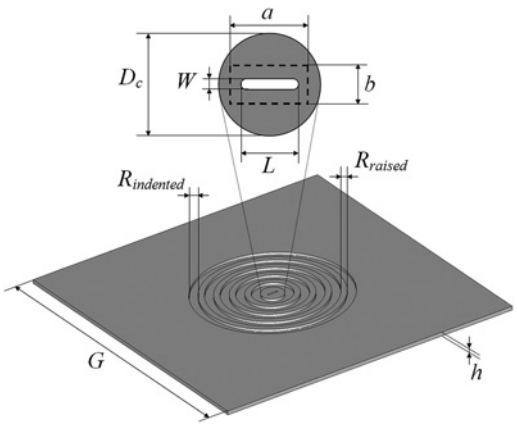

Fig. 1 *Design dimensions of the V-band Bull's eye antenna. The dotted line shows the position of the WR-15 waveguide feed*

eye antenna using a sectorial rotating plate in Section 5 and our conclusions in Section 6.

2 Single structure ring shift

In this section, we simulate the deflection of the main beam when the rings are shifted in a single direction. We begin by showing the effect, and then explain it in the later part of this section. The scheme for shifting the rings is as follows. The centre of each raised ring is shifted such that the n^{th} ring from the centre is shifted by $n \times Shift$, where *Shift* is the offset of the innermost raised ring. *Shift* is a free parameter in the limit that the rings can be produced in a conventional milling machine. This limits *Shift* to a maximum value of R_{indented}, which is 2.67 mm for our design in Table 1. Our shifting scheme retains the same dimension for the raised part of the ridge, but allows the indented portion to change size. This approach is preferable to the opposite approach (indented size stays the same size, raised ring changes size), which reduces the degree of shift, reduces the gain and introduces unwanted side lobes in the radiation pattern (results not shown here).

We carried out a parametric study in the *E* and *H* planes for *Shift* ranging from 0 to 2.67 mm, in seven steps (0, 0.50, 1.0, 1.5, 2.0, 2.5, 2.67 mm) to establish that the shifts are monotonic, but we present results only for shift of 0, 1.0, 2.0 and 2.67 mm for clarity in these figures in later sections. All our simulations are conducted with CST Microwave Studio's time-domain solver. The waveguide at the rear of the antenna is excited with a single-mode waveport and the metal is modelled as aluminium with conductivity of 3.538×10^7 S.m^{-1}. We use magnetic (or electric) walls for single or asymmetrical double shifts in the *E*-plane (or *H*-plane) to halve the simulation domain, and for symmetrical double shifts we use magnetic and electric walls to quarter the simulation domain. The far-field polar radiation patterns are plotted in Fig. 2 for *Shift* = 0 and 2.67 mm in the form of linear gain as a function of angle, with a perspective view of half of the associated Bull's eye structure. The purpose of Fig. 2 is to make clear the link between an offset in the rings and the deflection in the beam. Further details of the *E* and *H* planes shift can be found in [6].

The performance at some example intermediate deflections is summarised in Table 2. The deflection angle is approximately proportional to the *Shift* value, but the gain reduces from 18.1 to 13.5 dBi due to a slight increase in power radiated away from the main beam, rather than a change in the 3 dB beamwidth. Any secondary lobes remain below – 10 dBi, except when *Shift* = 2 mm

Table 1 Dimensions of the studied Bull's eye structure in millimetres

G	*a*	*b*	R_{indented}	R_{raised}	*W*	*L*	D_c	*h*
100	3.76	1.88	2.67	1.86	0.530	3.40	7.12	3.20

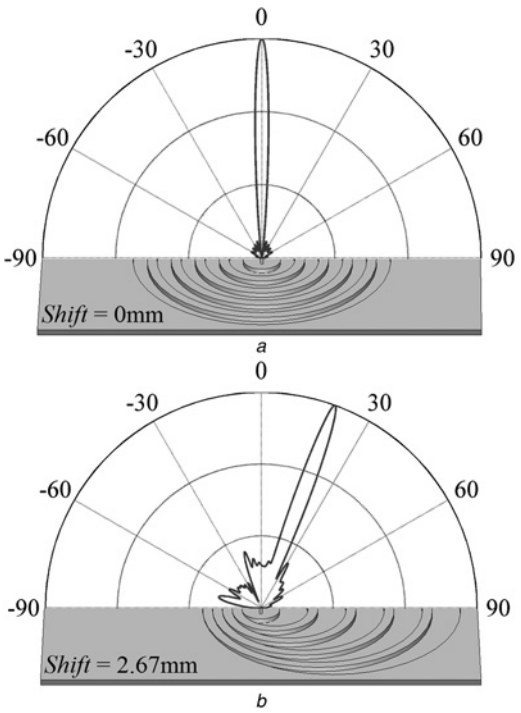

Fig. 2 *Qualitative illustration of how the Bull's eye antenna's main beam is deflected by shifting the rings. Each subfigure shows a polar plot of linear gain above a 3D view of half of the antenna*

a Standard design with unshifted rings yielding a single main beam directed along the broadside (maximum gain of 18.1 dBi)
b Design with shifted rings that deflects the single main beam by 20.0° (for a maximum gain of 13.5 dBi). In both cases the radiation efficiency is 97% and the aperture efficiency is 6%

(structure C), where an extra lobe at −25° rises at −6.8 dBi due to resonances in the surface currents (not shown here).

We attribute the beam deflection of shifted rings to the action of leaky waves [15]. To show that this explanation is consistent with our results, we compare the deflection angle of the main beam, to the coupling angle given by a standard momentum-matching equation. Momentum-matching equations are typically used to predict coupling angles for one-dimensional (1D) gratings in the optical regime and metal gratings in the microwave and millimetre-wave bands [16].

By considering the cross-section of our antenna along the main axis parallel to the direction of the shift, we can define a 1D grating that is approximately equivalent to our antenna. Naturally we do not expect this to represent accurately the behaviour of the antenna under all conditions. For example, we expect the 1D grating model to be less valid at larger shift values due to the loss of rotational symmetry, and the change in the effective filling factor. Nonetheless, a straightforward model helps elucidate the mechanism that dominates the antenna's performance. For a grating, the relationship between the surface wave phase constant β, the radiation angle θ and the period of the grating Λ is given by, for the $n = -1$ space harmonic

$$\beta = k_0 \sin\theta + \frac{2\pi}{\Lambda} \tag{1}$$

where $k_0 = 2\pi/\lambda_0$ is the free-space wavenumber. In this frequency range and since the grating is a good conductive metal, the surface

Table 2 Angle deflection and gain according to single *E*-plane ring shift

Ring shift, mm	0.0	0.50	1.0	1.5	2.0	2.5	2.67
deflection angle, deg	0.0	5.1	9.9	12.7	15.4	18.4	20.0
gain, dBi	18.1	18.4	17.9	16.5	16.6	13.4	13.5

wave phase constant is expected to be close to the free-space wavenumber $\beta \approx k_0$, and non-radiative (slow wave) with $\beta > k_0$.

Now we are interested in two questions: first, how good is a 1D grating model at predicting the performance of a Bull's eye antenna and second, what effect does the grating profile and filling factor have on the coupling angle? We address these two questions by plotting in Fig. 3 the deflection angle from a modified (optimised) and a canonical (un-optimised) Bull's eye antenna (modelled with CST Microwave Studio in 3D), their equivalent 1D gratings (modelled with Rigorous Coupled Wave Analysis [17]), and the deflection angle predicted for a sinusoidal grating of the same period. The sinusoidal grating is the black line, the (un-optimised) canonical grating and antenna are the black markers and the (optimised) modified grating and antenna are the white markers. Immediately it is clear that all five sets of results follow qualitatively the same trend. To emphasise the uniting role that leaky waves play in governing all the results that we present in Fig. 3, we plot, as a colourmap, surface wave phase constant β as a function of the effective grating period Λ, defined as the initial period Λ_0 plus the parameter *Shift* ($\Lambda = \Lambda_0 + Shift$), and the incident angle, by using (1). Aside from some deviation due to the rectangular grating profile and variable fill factor – which is known to affect the coupling angle [18] – and the extra dimension in the antenna rings versus a simple 1D grating.

To address the second question, we now discuss in more detail each of the sets of results in Fig. 3. As expected, the surface wave (non-radiative) has a phase velocity slightly lower than free space ($\beta > k_0$ and $\beta \approx k_0$). The 1D canonical grating (simulated by rigorous coupled-wave analysis (RCWA)) is remarkably close to the free-space wavenumber. The (un-optimised) canonical Bull's eye antenna ($\Lambda_0 = 5$ mm, filling factor = 0.50 to 0.33, black circles, shows a similar trend while showing discrepancies with the grating ranging from 0.7° to 2.98°, with an increasing trend (clearly visible from $\Lambda = 5.25$ to 6.5 mm) indicating the loss of rotational symmetry.

We plot as white markers, the deflection angle of the modified (optimised) grating ($\Lambda_0 = 4.53$ mm, filling factor = 0.41 to 0.26, white square markers) and the deflection angle of the modified (optimised) Bull's eye antenna ($\Lambda_0 = 4.53$ mm, filling factor = 0.41 to 0.26, white circle markers).

The modified grating's filling factor ranges from 0.41 to 0.26, creating narrower ridges with higher spatial harmonics than the canonical structure. We note that it is understood that β can vary slightly when the grating profile contains a significant amount of higher spatial harmonics [19], and we expect this to begin to strain the analogy to the 1D gratings at smaller shift values. The variation in β can be noted as a general trend that the reduction of the filling factor tends to increase the surface wave phase constant and subsequently the deflection angle.

Nonetheless, this simplified model is a useful way to understand the operation of the antenna, and gives an efficient approach to predicting the performance of a Bull's eye antenna, prior to conducting numerical simulations of optimised structures.

As expected, the surface wave (non-radiative) has a phase velocity slightly lower than free space ($\beta > k_0$), following an average isoline of $\beta = 1330$.

The *H*-plane shift has also been investigated and is reported in [6]. We only note here that the *E* and *H* plane shift performances are similar, allowing beam shifting even in polarisation diversity schemes where both *E* and *H* plane shifts are needed.

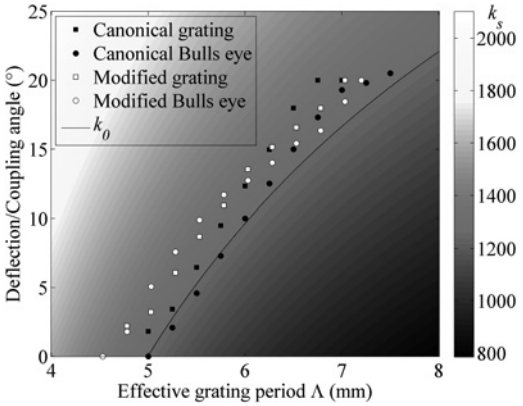

Fig. 3 *Plot comparing the simulated deflection angle of optimised ('modified') and un-optimised ('canonical') Bull's eye antennas to the coupling angle of the associated 1D rectangular profile gratings, as a function of the effective grating period $\Lambda = \Lambda_0 + shift$. The solid black line is the free-space wavenumber and the colourmap shows how the coupling angle and the grating period relate to the surface wave phase constant*

3 Double structure ring shift

We now explore the possibility of generating multiple main beams at one time. To do this, we put a different pattern on different sides of the antenna. This allows greater flexibility in future communications systems where more than one link is required simultaneously, yet with each individual link benefiting from a directive beam for power efficiency. The rest of this section is organised as follows. In Section 3.1, we first investigate symmetrical patterns so as to steer both beams equally, and then in Section 3.2 we investigate asymmetrical patterns so as to deflect each beam by a different amount.

3.1 Symmetrical shift

Two symmetrical structures have been investigated. The first has its ring centres shifted within the *E*-plane for positive-shift values. Fig. 4 shows the radiation patterns for *Shift* = 0, 1.0, 2.0 and 2.67 mm. Fig. 4(1) shows the creation of two primary separate lobes, with deflection angle ranging from 0° to 18.6°.

The gain drops from 18.1 to about 15.1 dBi, which is expected because of equal splitting of the power between the two main radiation beams (full efficiency is maintained overall). The secondary lobes stay below −8dBi. Table 3 shows the deflection angle, the maximum gain and the −3 dB beamwidth within the *E*-plane as a function of *Shift*.

We then investigated the *H*-plane positive double-shift structure for *Shift* = 0, 1.0, 2.0 and 2.67 mm. Fig. 5 shows the radiation pattern for the structure.

Two main lobes are still created, but the separation is not as obvious as for the *E*-plane until *Shift* ≥ 2 mm. Table 4 shows the deflection angle, the maximum gain and the −3 dB beamwidth within the *H*-plane according to the shift of the rings. If double lobes are required, the *E*-plane is preferable.

3.2 Asymmetrical shift

Since we established in the previous sections that the positive-shifted half of the *E*-plane pattern predominantly determines the beam properties, we expect that two different positive patterns can be combined to create beams that are deflected by different amounts. In other words, for *E*-plane positive shifts, each half of the pattern interacts with a different region of the surface current so we expect the beam deflection to be independently adjustable. This is desirable because it simplifies the design of an antenna to meet an arbitrary specification. We illustrate the independence of the two beams by example. We keep one beam along the normal direction (*Shift* = 0 mm) and progressively increase the deflection of the other beam by offsets of *Shift* = 0, 1.0, 2.0 and 2.67 mm. Fig. 6 shows the radiation patterns and plan view schematics of the ring patterns. The *E*-plane radiation patterns in Fig. 6(1) shows the deflection of the shifted lobe ranges from 0° to 21°.

Adding shift reduces the maximum gain to 10.1 dBi, for the maximally shifted lobe at *Shift* = 2.67 mm. On the other hand, the lobe that we did not want to deflect remains within −0.5° and 1.6° of the broadside. The gain of the line of sight lobe also drops from

IET Microw. Antennas Propag., 2016, Vol. 10, Iss. 3, pp. 318–325

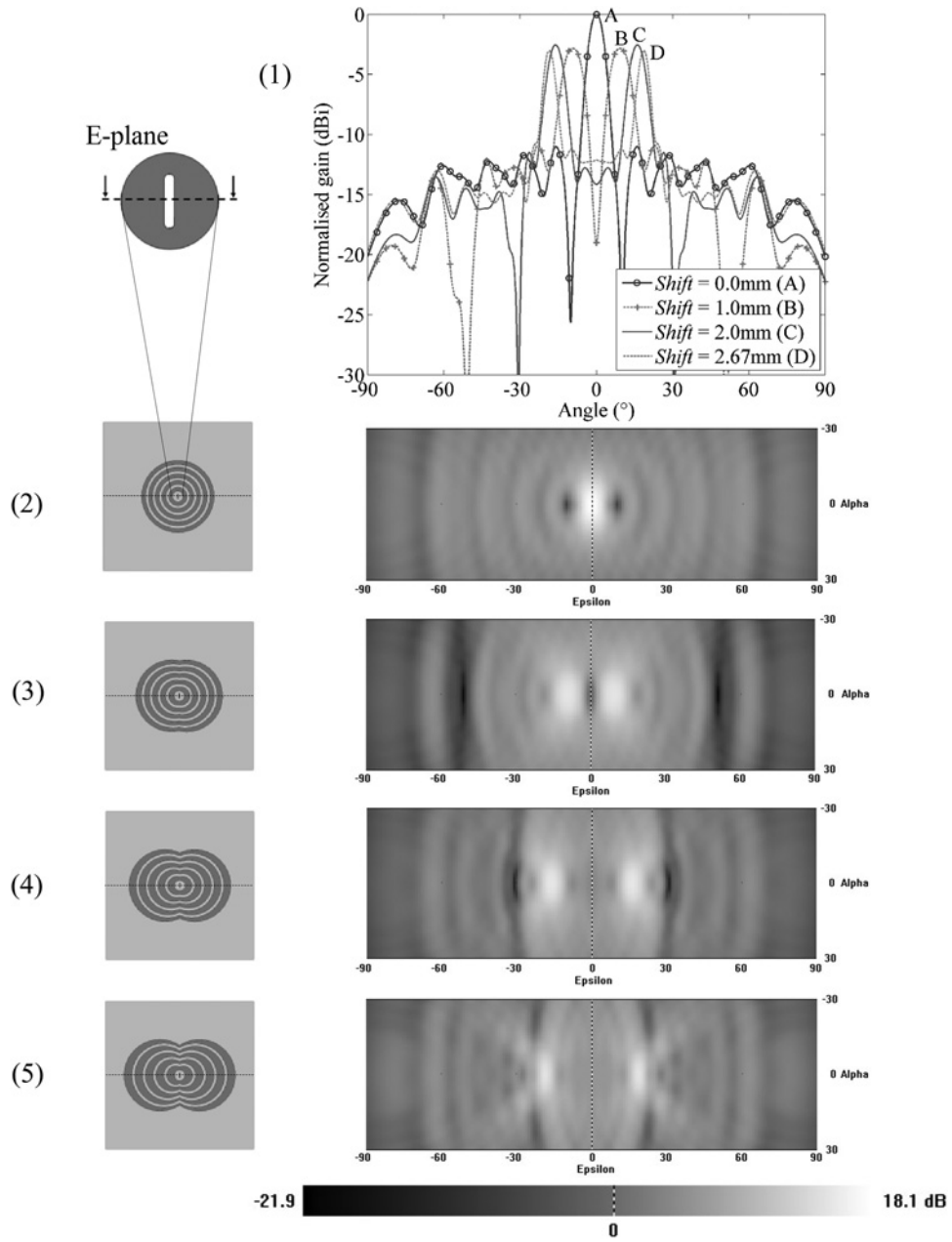

Fig. 4 *E-plane radiation patterns (1); and E-plane double positive-shift rings structure with corresponding 2D radiation pattern for 0.0 (2), 1.0 (3), 2.0 (4) and 2.67 mm (5) shift*

18.1 to 11.6 dBi, as shown in Fig. 6(1). We attribute this to a small interaction of the currents on each side of the aperture. We did not optimise this design further, but we suggest introducing small un-patterned guard bands or trenches, between the two gratings.

4 Measurements

To experimentally demonstrate that multiple beams can be created, as we have proposed here, we manufactured an *E*-plane double positive-shift Bull's eye antenna with *Shift* = 2.0 mm, for an expected deflection of 16.1° on each side of the broadside. A three-axis *XYZ* SM2000 computer numerical control (CNC) milling machine was used to create ring pattern on the aluminium plate. We measured the antenna radiation pattern inside a 4.5 m × 4.5 m × 4.0 m anechoic antenna test chamber so as to avoid electromagnetic interference and parasitic reflections. The structure was mounted on a rotating stage taking measurements from −90° to +90°, in steps of 2°. Experimental *S*21 parameter data was acquired via an Agilent performance network analyses (PNA) (E8361A) with 500 Hz intermediate frequency (IF) bandwidth and averaging of ten points per sample, with a linearly polarised 23 dBi horn antenna (Custom Microwave, Inc., model HO15R), separated by 110 cm (220λ) from the Bull's eye antenna under test. Fig. 7*a* shows a photograph of the fabricated 2 mm *E*-plane shift Bull's eye antenna and Fig. 7*b* shows the simulated and measured *E*-plane radiation patterns, after normalisation.

Fig. 7*b* shows good agreement between the two normalised *E*-plane radiation patterns. The measured main lobe on the negative angle side is offset by −2° from the simulation, while

Table 3 Deflection angle, gain and beamwidth according to double *E*-plane positive ring shift

Ring shift, mm	0.0	1.0	2.0	2.67
deflection angle, deg	0.0	9.3	16.1	18.6
gain, dBi	18.1	15.3	15.6	15.1
−3 dB beamwidth, deg	6.7	8.9	7.3	5.1

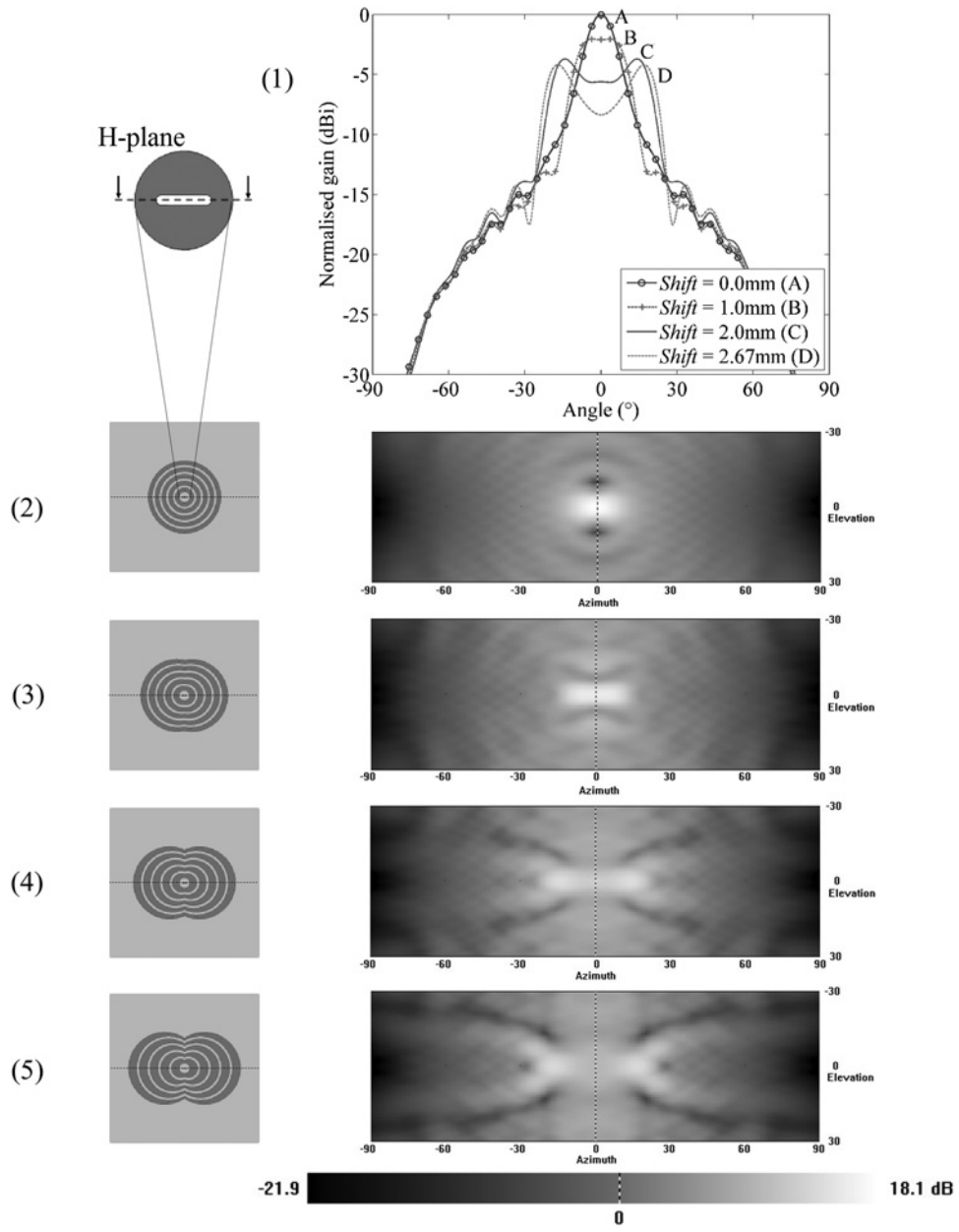

Fig. 5 *H-plane radiation patterns (1); and H-plane double positive-shift rings structure with corresponding 2D radiation pattern for 0.0* (2)*, 1.0 (3), 2.0 (4) and 2.67 mm (5) shift*

there is good agreement in the location of the secondary lobes at ±39°, ±52°, ±64° and ±80°, and nulls at ±30°. We attribute the small shift in the main lobe to fabrication tolerances in the production of the antenna.

5 Mechanical steering with sectorial structure

A beam steering capability is essential for point-to-point communications where there are multiple transceivers (such as consumer products in a domestic environment or a constellation of small satellites or CubeSats in space). Electronic beam steering via phased arrays such as [20, 21] is often fast, and ideal for short range communication where the environment varies rapidly, but the link budget is not strained. However, electronic beam steering introduces losses through networks of splitters and phase shifters or delay lines [22]. A typical electronic phase shifter can introduce up to 3 dB of insertion loss, reducing range by 30% for a given link budget. To counter this, mechanical steering systems have been proposed such as mechanically tilting dielectric lenses [23], though these introduce a coupling loss between the feed horn and the lenses which is not present in a Bull's eye design.

For applications such as mobile backhaul, point-to-point communication in fixed (or reconfigurable) constellations of small satellites, and millimetre-wave radar, the overall link budget is often constrained. It is necessary to prioritise range and signal-to-noise ratio over speed of beam steering. For example, the orbital low frequency ARay (OLFAR) CubeSat mission [24] can use the 59–71 GHz intersatellite service band for high bandwidth data-sharing between swarm members. Power budgets are strictly limited by the small size of the platform and therefore the higher

Table 4 Deflection angle, gain and beamwidth according to double *H*-plane positive ring shift

Ring shift, mm	0.0	1.0	2.0	2.67
deflection angle, deg	0.0	3.3	14.3	17.0
gain, dBi	18.1	16.0	14.4	13.9
beamwidth, deg	13.2	22.1	40.3	15.2

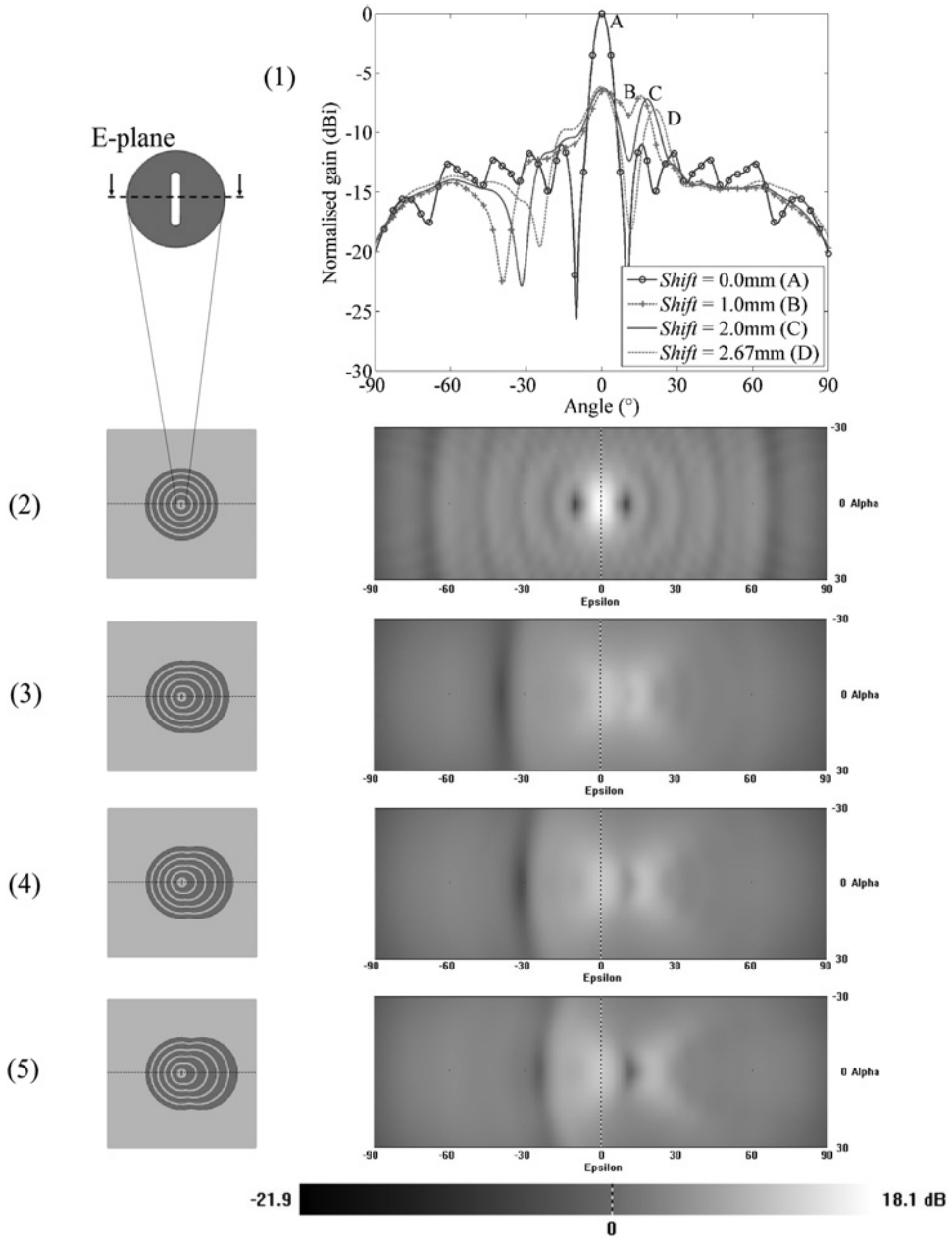

Fig. 6 *E-plane radiation patterns (1); and E-plane asymmetrical shift rings structure with corresponding 2D-projection radiation pattern for 0.0 (2), 1.0 (3), 2.0 (4) and 2.67 mm (5) shift*

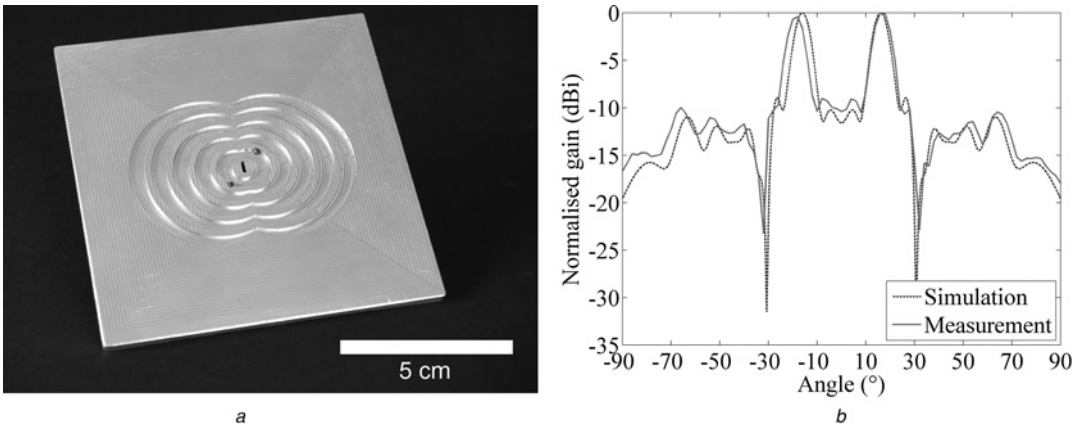

Fig. 7 *Measurements of E-plane double positive-shift Bull's eye antenna with shift = 2.0 mm*

a Fabricated Bull's eye antenna prototype
b Normalised simulated and measured *E*-plane radiation pattern

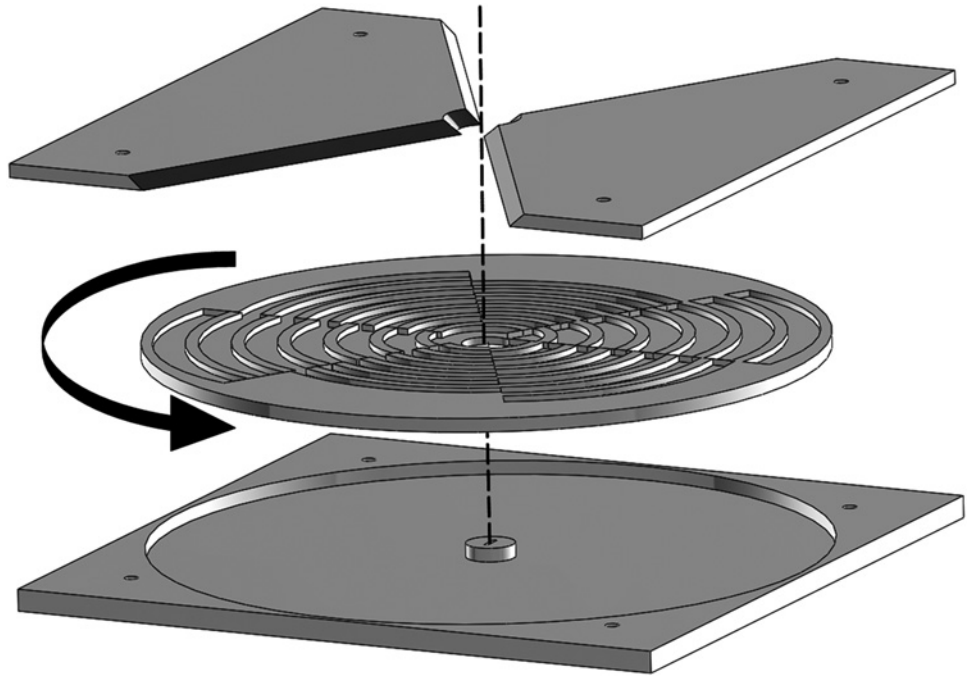

Fig. 8 *Exploded view of the six-sector mechanical shift antenna with rotating plate*

transmission efficiency of a mechanical steering system is attractive because it allows the CubeSat constellation to cover a wider area yet still share high-bandwidth data.

For the Bull's eye antenna, a number of mechanical steering schemes are apparent – but most suffer from severe disadvantages in practice. For example, attempting to create individually machined moving rings results in a complex mechanism that offsets any cost or space saving associated with the fixed version of the design. Instead we propose to sacrifice continuous tunability for a mechanically straightforward scheme with few moving parts.

Fig. 8 shows the exploded view of our concept, which comprises three parts: an aluminium mask, a rotating plate with six sectors (60° each) each containing different ring patterns, and a fixed aluminium base including the subwavelength aperture. The aluminium mask is necessary to counterbalance the effect of an asymmetrical pattern along the unsteered-plane for each of the positions, i.e. for an antenna that steers in the *E*-plane, these sections of the antenna that would influence the *H*-plane should be masked, and vice versa. The system for rotating the sectorial plate is not shown here, for simplicity. We suggest adding teeth to the outer teeth of the sectorial plate and using a geared drive to rotate it. Ball races can be built into the interface between the base and the sectorial plate, which will prevent friction without disrupting any surface current flows because they will be away from the active surfaces.

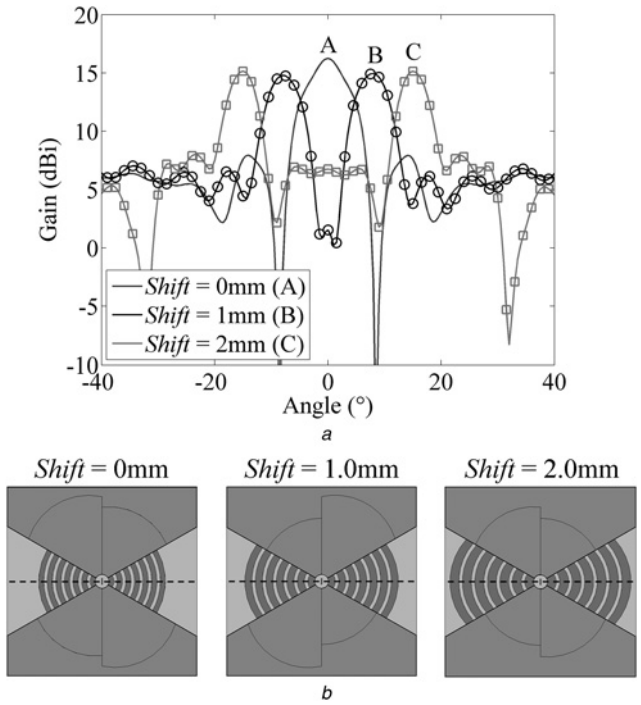

Fig. 9 *Simulation results for the six-sector mechanical shift structure antenna*

a *E*-plane radiation pattern for the three positions (0, 1 and 2 mm shifts)
b Corresponding structures (mask showed in transparency), where the dotted line represents the *E*-plane

Fig. 9 shows the simulated *E*-plane radiation pattern for the three positions (a), with corresponding structures (b). Fig. 9*b* also illustrates asymmetry of the structure on each side of the *E*-plane. The three positions (*Shift* = 0, 1 and 2 mm) provide main beam deflection of 0°, ±7.9° and ±15.0° within the *E*-plane and a maximum gain of 16.2, 14.9 and 15.1 dBi.

In results not shown here, we also designed a sectorial plate that allowed a single beam to be steered to −14.5°, −7.7°, 0°, +7.7° and +14.5°, with a maximum gain of 17.1 dBi at ±7.7°.

6 Conclusion

We presented the design of Bull's eye antennas with deflected double beams in the *E* and *H* planes, and a mechanical scheme for making single and double beams discretely steerable during operation. We deflected the beam(s) by shifting the rings that surround the aperture. For a shift of 2.67 mm in the *E*-plane, a single beam is deflected by 20°, yet retained a high-gain narrow beam (18.1 dBi for an undeflected beam, 13.5 dBi for a fully deflected beam) and a high radiation efficiency (97%). We explained the operation of the antenna in terms of leaky wave, showing that a simple 1D grating model is sufficient to predict the deflection angle with minimal computational effort and reasonable accuracy. Since leaky wave coupling are a localised effect, it is possible to independently design different gratings on different sides of the aperture, with each grating setting the deflection angle

IET Microw. Antennas Propag., 2016, Vol. 10, Iss. 3, pp. 318–325

of its own beam. We experimentally validated this concept for an antenna that created two beams deflected to 16.1° either side of the broadside, with a gain of 15.6 dBi. Fixed designs could be useful in a number of static scenarios, but a steerable antenna would give more flexibility. While a number of mechanical steering schemes are possible for this type of antenna, many are likely to be mechanically impractical. We proposed a straightforward scheme based on a rotating plate with different patterns in six sectors, and a mask to prevent unwanted modifications to the beam-shape by the inactive portions of the sectorial plate. In the example design we presented, we can select between a single beam along the broadside or two beams at either 7.9° or 15.0°. In another version, that we did not show, we could deflect a single beam to −14.5°, −7.7°, 0°, +7.7° or +14.5°, i.e. five different directions. The choice of angles is arbitrary. In summary, the Bull's eye antenna is compact, inexpensive and flexible and we expect it to be useful in point-to-(multi-)point links in terrestrial and space-based applications.

7 Acknowledgments

We thank the staff of the University of Glasgow's mechanical workshop for making the Bull's eye antenna. Timothy D. Drysdale acknowledges support from European 7th research framework programme (EU FP7) International Research Staff Exchange (ISRES) project Advanced Methods for Analyzing and Improving the Reliability of Things (AdvIOT). Clement J. Vourch acknowledges support from the University of Glasgow James Watt Research Scholarship.

8 References

1 Lezec, H.J., Degiron, A., Devaux, E., *et al.*: 'Beaming light from a subwavelength aperture', *Science 2*, 2002, **297**, (5582), pp. 820–822
2 Beruete, M., Campillo, I., Dolado, J.S., *et al.*: 'Very low-profile 'Bull's eye' feeder antenna', *IEEE Antennas Wirel. Propag. Lett.*, 2005, **4**, pp. 365–368
3 Beruete, M., Beaskoetxea, U., Zehar, M., *et al.*: 'Terahertz corrugated and Bull's-eye antennas', *IEEE Trans. Terahertz Sci. Technol.*, 2013, **3**, (6), pp. 740–747
4 Beaskoetxea, U., Pacheco-Pena, V., Orazbayev, B., *et al.*: '77 GHz high-gain Bull's-eye antenna with sinusoidal profile', *IEEE Antennas Wirel. Propag. Lett.*, 2015, **14**, pp. 205–208
5 Tetienne, J., Blanchard, R., Yu, N., *et al.*: 'Dipolar modeling and experimental demonstration of multi-beam plasmonic collimators', *New J. Phys.*, 2011, **13**, (5), pp. 1–8
6 Vourch, C.J., Drysdale, T.D.: 'V-band 'Bull's eye' antenna for CubeSat applications', *IEEE Antennas Wirel. Propag. Lett.*, 2014, **13**, pp. 1092–1095
7 Minatti, G., Sabbadini, M., Maci, S.: 'Surface to leaky wave transformation in polarized metasurfaces'. Proc. of 2013 URSI Int. Symp. on Electromagnetic Theory (EMTS), 20–24 May 2013, pp. 298–301
8 Minatti, G., Faenzi, M., Martini, E., *et al.*: 'Modulated metasurface antennas for space: synthesis, analysis and realizations', *IEEE Trans. Antennas Propag.*, 2015, **63**, (4), pp. 1288–1300
9 ElSherbiny, M., Fathy, A.E., Rosen, A., *et al.*: 'Holographic antenna concept, analysis and parameters', *IEEE Trans. Antennas Propag.*, 2004, **52**, (3), pp. 830–839
10 Rusch, C.: 'Holographic antennas', in Cheng, Z.N. (ED.): 'Handbook of antenna technologies' (Springer, 2015), pp. 1–31
11 International Telecommunication Union, Recommendation ITU-R P.531–12: 'Ionospheric propagation data and prediction methods required for the design of satellite services and systems', September 2013
12 Jehle, M., Ruegg, M., Zuberbuhler, L., *et al.*: 'Measurement of ionospheric Faraday rotation in simulated and real spaceborne SAR data', *IEEE Trans. Geosci. Remote Sens.*, 2009, **47**, (5), pp. 1512–1523
13 Ng, K.B., Wong, H., So, K.K., *et al.*: '60 GHz plated through hole printed magneto-electric dipole antenna', *IEEE Trans. Antennas Propag.*, 2012, **60**, (7), pp. 3129–3136
14 Li, Y., Luk, K.:'A 60 GHz dense dielectric patch antenna array', *IEEE Trans. Antennas Propag.*, 2014, **62**, (2), pp. 960–963
15 Jackson, D.R., Caloz, C., Itoh, T.: 'Leaky-wave antennas', *Proc. IEEE*, 2012, **100**, (7), pp. 2194–2206
16 Hibbins, A.P., Sambles, J.R., Lawrence, C.R.: 'Grating-coupled surface plasmons at microwave frequencies', *J. Appl. Phys.*, 1999, **86**, (4), pp. 1791–1795
17 Moharam, M.G., Gaylord, T.K.: 'Rigorous coupled-wave analysis of metallic surface-relief gratings', *J. Opt. Soc. Am. A*, 1986, **3**, (11), pp. 1780–1787
18 Giannattasio, A., Hooper, I.R., Barnes, W.L.: 'Dependence on surface profile in grating-assisted coupling of light to surface plasmon-polaritons', *Opt. Commun.*, 2006, **261**, (2), pp. 291–295
19 Raether, H.: 'Surface plasmons on smooth and rough surfaces and on gratings' (Springer Tracts in Modern Physics, Springer Berlin, 1988), vol. 111
20 Emami, S., Wiser, R.F., Ali, E., *et al.*: 'A 60 GHz CMOS phased-array transceiver pair for multi-Gb/s wireless communications'. IEEE Int. Solid-State Circuits Conf. Digest of Technical Papers (ISSCC), 20–24 February. 2011, pp. 164–166
21 Natarajan, A., Reynolds, S.K., Ming-Da, T., *et al.*: 'A fully-integrated 16-element phased-array receiver in SiGe BiCMOS for 60 GHz communications', *IEEE J. Solid-State Circuits*, 2011, **46**, (5), pp. 1059–1075
22 Ta, C.M., Skafidas, E., Evans, R.J., *et al.*: 'A 60 GHz variable delay line on CMOS for steerable antennae in wireless communication systems'. Canadian Conf. on Electrical and Computer Engineering, 4–7 May 2008, pp. 1915–1918
23 Costa, J.R., Lima, E.B., Fernandes, C.A.: 'Compact beam-steerable lens antenna for 60 GHz wireless communications', *IEEE Trans. Antennas Propag.*, 2009, **57**, (10), pp. 2926–2933
24 Rajan, R.T., Engelen, S., Bentum, M., *et al.*: 'Orbiting low frequency array for radio astronomy'. IEEE Aerospace Conf., 5–12 March 2011, pp. 1–11